Supplementary Information (SI) for Green Chemistry.
This journal is © The Royal Society of Chemistry 2025

Supplementary information

MOF-Derived Cobalt Catalysts for Sustainable Tandem Hydroformylation–Acetalization in Green Solvents: Experimental and DFT Calculations

Wejdan Hadi Anbari [a†], Leandro Duarte Almeida [a†], Alejandra Rendón Patiño [a], Rafia Ahmad [b], Luis Garzon-Tovar [a], Luigi Cavallo [b] and Jorge Gascon [a]*

[a] Advanced Catalytic Materials (ACM), KAUST Catalysis Center (KCC), King Abdullah University of Science and Technology (KAUST), Thuwal 23955-6900, Saudi Arabia

[b] KAUST Catalysis Center (KCC), King Abdullah University of Science and Technology (KAUST), Thuwal 23955-6900, Saudi Arabia

[†] These authors contributed equally to this work

* Corresponding author: jorge.gascon@kaust.edu.sa

Table of Contents

Characterizations 4

Synthesis of pyrolyzed MOF-74 7

Results 8

Figure S1. (a) PXRD, (b) TGA under N2, (c) N2 adsorption isotherm, (d) Brunauer-Emmett Teller (BET) fit, (e) SEM image, and (f) average crystal size for ZIF-67. 8

Figure S2. TEM images of fresh Co@C_{600} 9

Figure S3. High-angle annular dark-field scanning transmission electron microscopy (HAADF-STEM) of the fresh Co@C_{600} 10

Figure S4. Thermogravimetric analysis under air of the cobalt pyrolyzed catalyst Co@C_{600} 11

Table S1. TGA, CHN elemental composition, and hydrogen chemisorption data of the synthesized cobalt-based material 12

Figure S5. N_2 adsorption isotherms and Brunauer-Emmett Teller (BET) fits for Co@C_{600} 13

Figure S6. C 1s, N 1s, and Co 2p XPS spectra of Co@C_{600} 14

Table S2. Percentage of deconvoluted peaks in N 1s XPS spectra 14

Table S3. Percentage of deconvoluted peaks in C 1s XPS spectra 14

Table S4. Percentage of deconvoluted peaks in Co 2p XPS spectra 15

Figure S 7. NH_3-TPD of Co@C_{600} catalyst 16

Table S5. Optimization of the reaction conditions for the tandem hydroformylation-acetalization of 1-octene 17

Figure S 8. (a) 1-octene reaction rate and (b) monitoring of octenes formation. Conversion and yield were determined by GC using mesitylene as the internal standard 19

Figure S 9. Kinetic isotope effect experiments with CH_3OH and CD_3OD. (a) 1-octene consumption, (b) formation of internal octenes, (c) acetals and aldehydes yields, and (d) linear-to-branched ratio formation of acetals. 20

Figure S10. Hot filtration experiment with the (a) Co@C_{600} and (b) pyrolyzed MOF-74 catalysts. 21

Figure S 11. PXRD of (a) MOF-74 and (b) its pyrolyzed material, (c) cobalt particle size distribution and (d-f) TEM images of pyrolyzed MOF-74.....22

Figure S12. Nonanal adsorption on Co and CoO on supports (Graphene, CN and pCN).....23

Figure S13. 2-Methyloctanal adsorption on Co and CoO on supports (Graphene, CN and pCN).....23

Figure S 14. Element-resolved projected density of states (PDOS) for Co nanoparticles (Co NP) supported on graphene, nitrogen-doped graphene (CN), and porous carbon nitride (pCN) before and after adsorption of nonanal and 2-methyloctanal. 24

Figure S 15. Element-resolved projected density of states (PDOS) for CoO nanoparticles (CoO NP) supported on graphene, nitrogen-doped graphene (CN), and porous carbon nitride (pCN) before and after adsorption of nonanal and 2-methyloctanal. 25

Figure S 16. Changes in Bader charge (Δ charge = adsorbed − free/base) for selected atoms during adsorption of nonanal (left) and 2-methyloctanal (right) on Co and CoO nanoparticles supported on nitrogen-doped graphene (CN). 26

Figure S 17. (a) TGA and (b) Raman spectroscopy of fresh and used Co@C_{600} catalyst.....27

Figure S18. TEM images of used Co@C_{600} 28

Figure S19. Cobalt particle size distribution of the used Co@C_{600} catalyst 29

Figure S20. High-angle annular dark-field scanning transmission electron microscopy (HAADF-STEM) of the used Co@C_{600} after five cycles 30

Table S6. Elemental quantification by XPS 31

Figure S21. C 1s, N 1s, and Co 2p XPS spectra of the used Co@C_{600} catalyst. 31

Table S 7. O 1s XPS deconvolution data 32

Figure S 22. O 1s XPS spectra of (a) fresh and (b) used Co@C_{600} catalyst 32

References.....33

Characterizations

Powder X-ray Diffraction (PXRD): X-ray diffraction measurements were conducted in a Bruker D8 Advance diffractometer in Bragg-Brentano geometry fitted with a copper tube operating at 40 kV and 40 mA. The ZIF-67 data was acquired from 4-30°, using a step size of 0.018° with a time per step of 192 s. The pyrolyzed materials were analysed from 15-70°, using a step size of 0.0204° with time per step of 4.9 s.

Thermogravimetric Analysis (TGA): The measurements were performed using a Mettler Toledo TGA/DSC equipment employing a 30 µL platinum crucible. The heating rate was set to 10 °C min^{-1}, with a constant flow of air or nitrogen at 20 mL min^{-1}.

Scanning Electron Microscopy (SEM): Images of the sample were obtained using a field emission scanning electron microscope Zeiss Merlin instrument, operating at a constant acceleration voltage of 5 kV and a current of 1.2 nA. The sample was coated with a 5 nm Iridium layer before measurement.

CHN Elemental analysis: The analysis were performed in a Flash Smart OEA elemental analyzer with a MAS autosampler from Thermo Fisher Scientific. The gases flow rate was 140 mL min^{-1} for helium, 100 mL min^{-1} for reference gas, and 250 mL min^{-1} for oxygen. Injection end time. The sample was processed in the presence of excess O_2 by flash combustion. The gaseous products were carried in a helium flow through reduced copper wire held at ca 950 °C. The gas products were separated in a gas chromatography column before entering the TCD detector.

Adsorption/desorption of N_2: N_2 adsorption-desorption measurements were performed at 77 K using a Micromeritics ASAP 2040 instrument. Before measurements samples were degassed at 120 °C for 12 h under vacuum.

Raman Spectroscopy: The analysis was performed in a Witec Apyron equipment using a 532 nm laser, power of 1 mW, integration time of 5 seconds, and accumulation of 50.

Hydrogen chemisorption: Chemisorption experiments were conducted using a Micromeritics ASAP2020 instrument with Grade 5 Hydrogen. Approximately 40 mg of the sample was utilized in each experiment, supported on quartz wool within a flow-through sample tube. The samples were degassed at 120 °C under vacuum for 2 hours, reduced with H_2 at 400 °C for 120 minutes, and cooled down to room temperature under helium. The analysis was conducted at 140 °C with a heating rate of 10 °C min^{-1} and 20 minutes per step.

X-ray Photoelectron Spectroscopy (XPS): X-ray photoelectron spectra were acquired using an Amicus instrument (Kratos Analytical), employing Al Kα radiation with an energy of 1486.6 eV. The excitation source operated within an ultrahigh vacuum environment, with a pressure of 6.7×10^{-8} Pa. Binding energies (BE) were calibrated using the adventitious carbon C 1s BE reference point of 284.8 eV. The XPS spectra were deconvoluted and fitted by a Gaussian and Lorentzian function with the CasaXPS 2.3 software.

Transmission Electronic Microscopy (TEM): Transmission electron microscopy imaging was conducted using a Titan ST instrument (FEI Company) operating at 300 keV. High-angle annular dark field–scanning transmission electron microscopy (HAADF–STEM) images were captured with a Cs-probe-corrected Titan microscope (FEI Company) operating at an accelerating voltage of 300 kV. Dark-field images were obtained using a STEM instrument equipped with a HAADF detector. Elemental distributions via energy-dispersive X-ray spectroscopy (EDX) were mapped in weight percent (wt %) and subjected to smooth post-filtering using a Gaussian filter (sigma = 0.9) through Velox Software. All TEM samples were prepared on dry copper grids coated with a lacey Carbon film (300 mesh).

Ammonia temperature programmed desorption (NH_3-TPD): The analysis was performed in a Micromeritics AutoChem III 2930 equipment. The sample was dried under Ar at 150 °C for 1 hour before the analysis. Ammonia was adsorbed using 10% NH_3/Ar at 50 °C for 60 minutes under 50 mL min^{-1} flow,

followed by inert gas flush for 30 minutes. The desorption step was realized with a heating rate of 10 °C min^{-1} until 650 °C.

Synthesis of pyrolyzed MOF-74

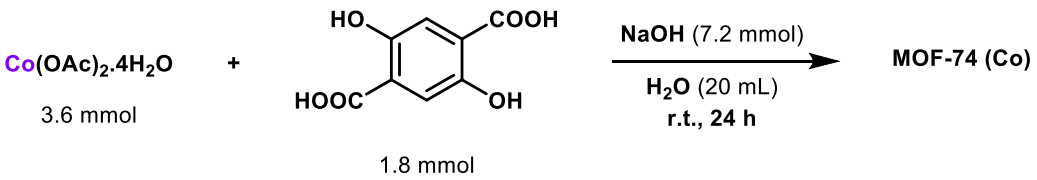

Synthesis of pristine MOF-74 (Co): The MOF-74 was prepared according to previously reported procedure.[1] An aqueous solution (5 mL) of NaOH (0.288 g) and 2,5-dihydroxyterephthalic acid (0.357 g) was prepared, and mixed with an aqueous (15 mL) cobalt acetate (0.897 g) solution. The resulting mixture was magnetically stirred (400 rpm) at room temperature for 24 hours. The final powder was recovered by centrifugation and washed with water (3x25 mL) and methanol (3x25 mL), then dried at 65 °C overnight.

Pyrolysis of MOF-74: The procedure is the same as described for the pyrolysis of ZIF-67. The pyrolysis process was conducted using a quartz tubular reactor positioned vertically within a tube furnace. MOF-74 was placed inside the reactor, and with a continuous flow of N_2 (30 mL min^{-1}), it was subjected to heating at 600 °C for 6 hours at a heating rate of 2 °C min^{-1}. After cooling down below 50 °C, the materials were passivated under a flow of air (20 mL min^{-1}) for 2 hours.

Results

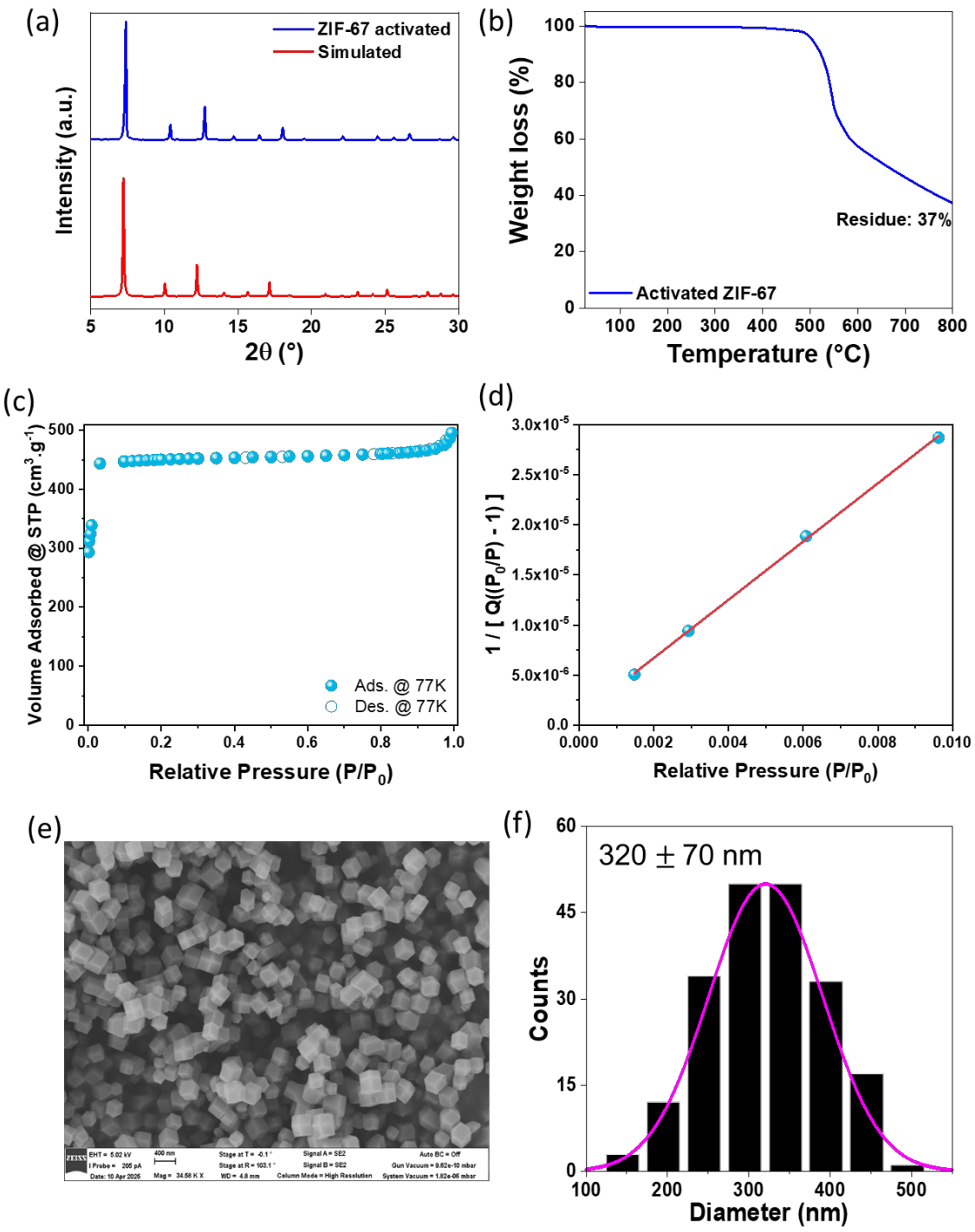

Figure S1. (a) PXRD, (b) TGA under N2, (c) N2 adsorption isotherm, (d) Brunauer-Emmett Teller (BET) fit, (e) SEM image, and (f) average crystal size for ZIF-67.

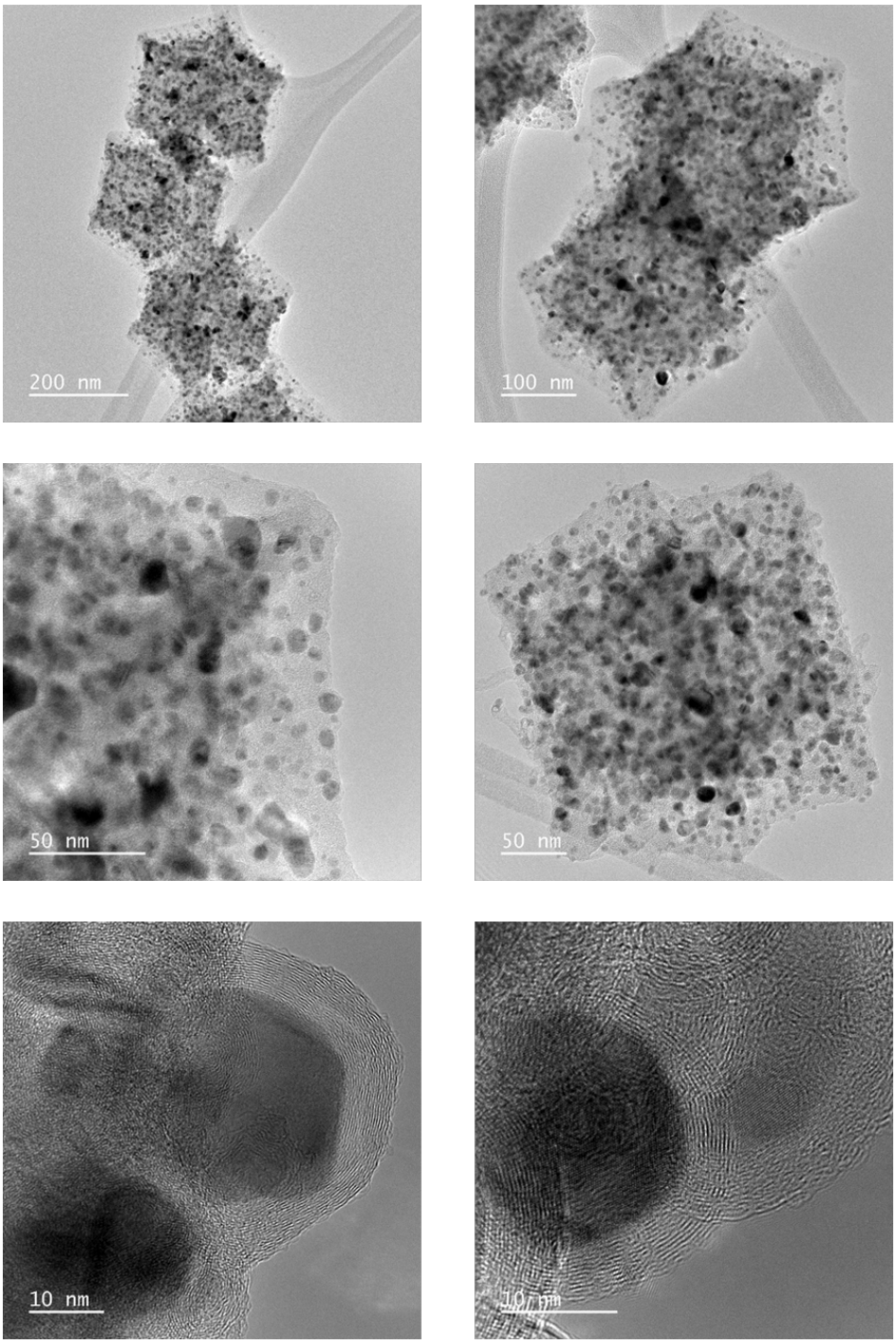

Figure S2. TEM images of fresh Co@C_{600}

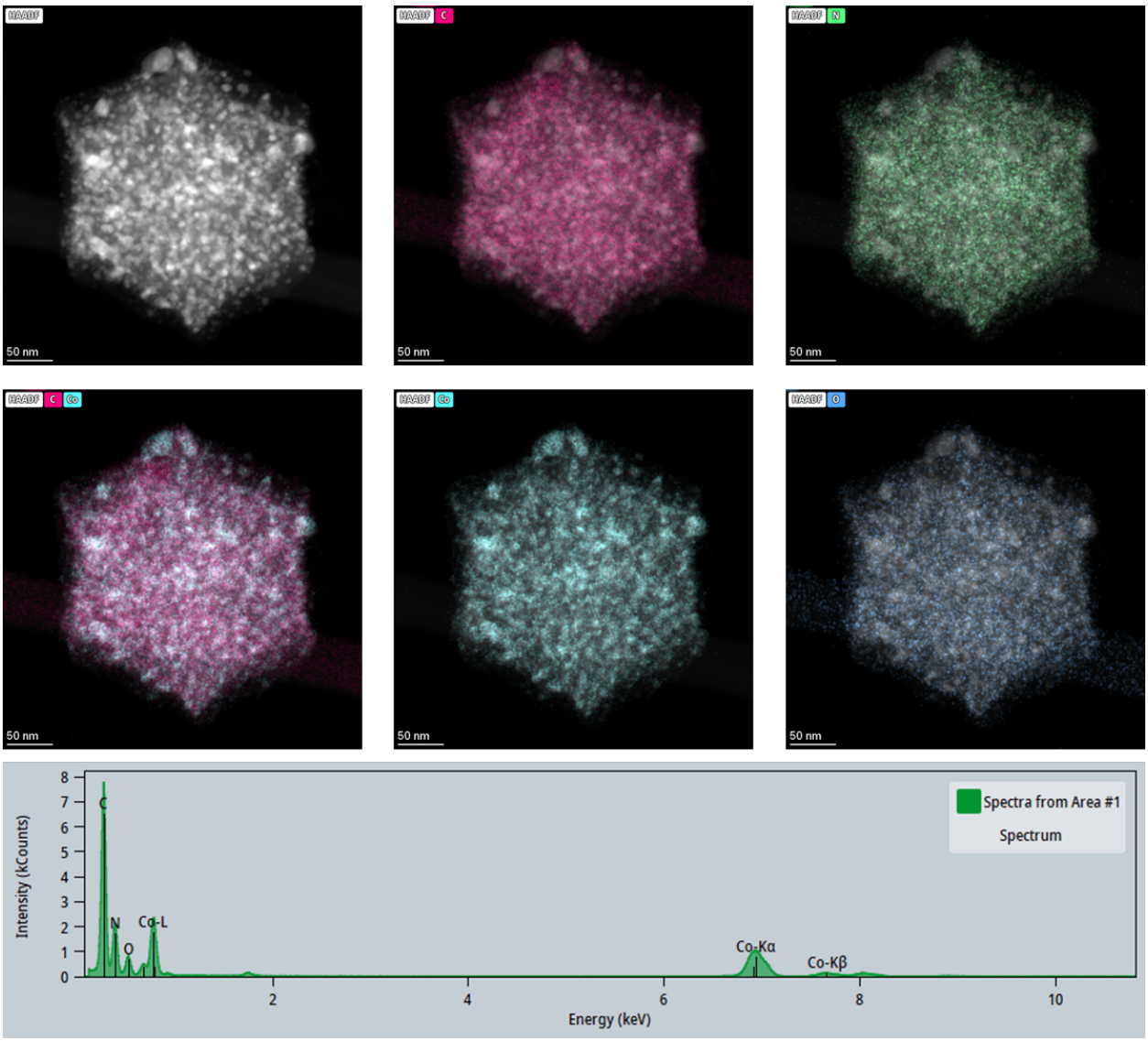

Figure S3. High-angle annular dark-field scanning transmission electron microscopy (HAADF-STEM) of the fresh Co@C_{600}

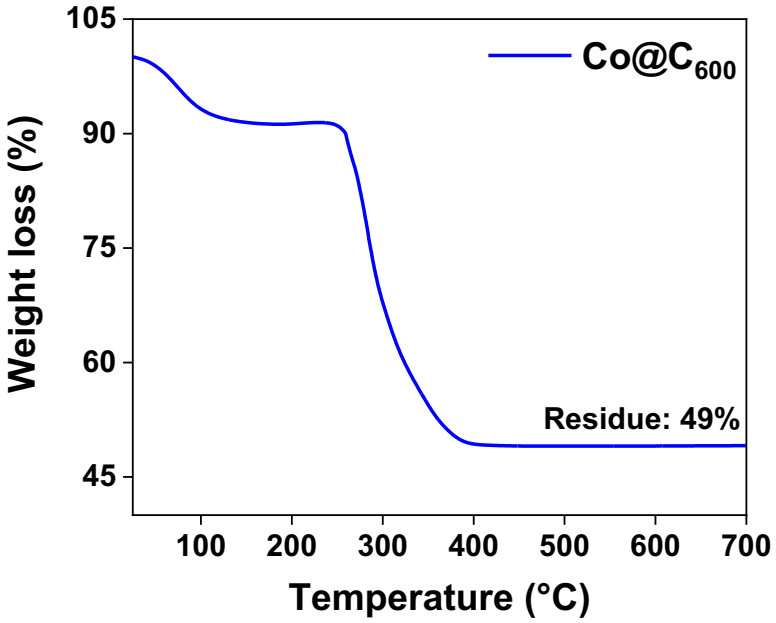

Figure S4. Thermogravimetric analysis under air of the cobalt pyrolyzed catalyst Co@C_{600}

Table S1. TGA, CHN elemental composition, and hydrogen chemisorption data of the synthesized cobalt-based material

	Elemental analysis (%)					Metal	Metallic surface area
Sample	**Co [a]**	**C [b]**	**N [b]**	**H [b]**	**Total (%)**	**dispersion (%) [c]**	**(m^2 g^{-1} of sample) [c]**
$Co@C_{600}$	36	39.2	12.4	1.3	88.9	2.22	5.41

[a] Determined by TGA

[b] Determined by CHN

[c] Determined by H_2 chemisorption

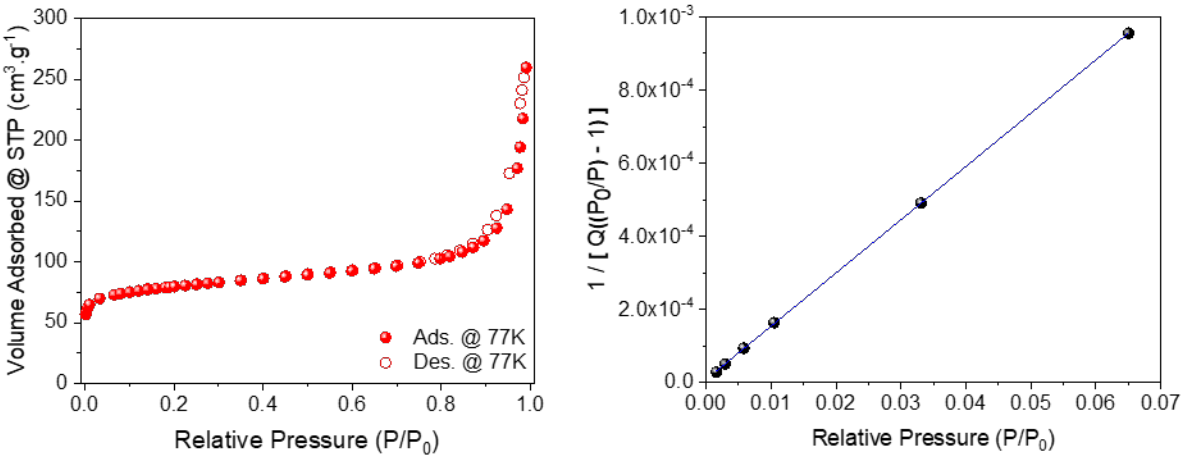

Figure S5. N_2 adsorption isotherms and Brunauer-Emmett Teller (BET) fits for $Co@C_{600}$

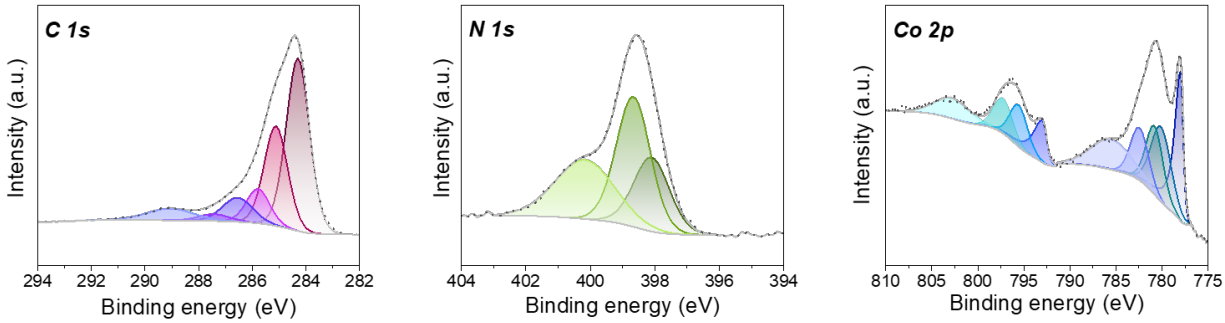

Figure S6. C 1s, N 1s, and Co 2p XPS spectra of Co@C_{600}

Table S2. Percentage of deconvoluted peaks in N 1s XPS spectra

N 1s	Co@C_{600}	Used 5x Co@C_{600}
Pyridinic N	21.9	25.0
Pyrrolic N	38.5	41.9
Graphitic N	39.6	33.1

Table S3. Percentage of deconvoluted peaks in C 1s XPS spectra

C 1s	Co@C_{600}	Used 5x Co@C_{600}
C=C	51.8	46.6
C-C	25.4	26.9
C-N/C=N	8.70	9.26
C-O	5.40	8.40
C=O	3.40	2.48
O-C=O	5.30	6.34

Table S4. Percentage of deconvoluted peaks in Co 2p XPS spectra

Co 2p		Co@C_{600}	Used 5x Co@C_{600}
Co $2p_{3/2}$	Co(0)	18.0	13.6
	Co(III)	17.2	13.0
	Co(II)	13.7	19.9
	Sat.	11.4	7.8
	Sat.	13.5	14.0
Co $2p_{1/2}$	Co(0)	7.4	5.0
	Co(III)	7.9	6.4
	Co(II)	6.1	9.0
	Sat.	4.8	11.3

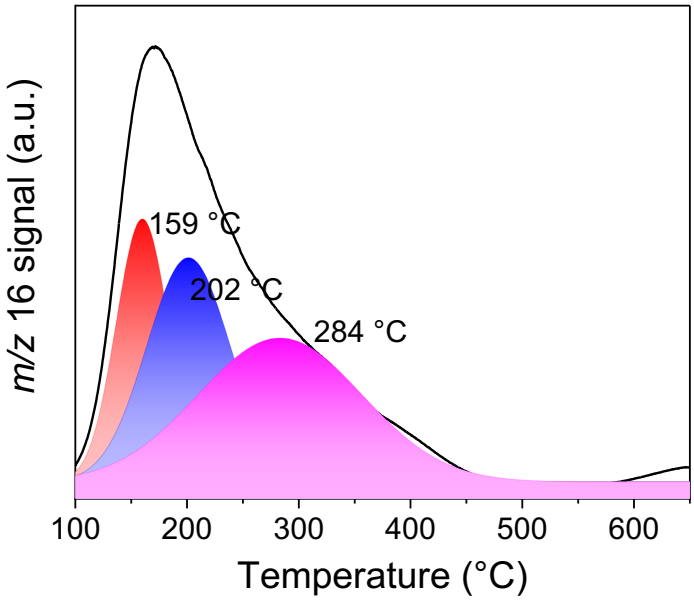

Figure S 7. NH_3-TPD of Co@C_{600} catalyst

Table S5. Optimization of the reaction conditions for the tandem hydroformylation-acetalization of 1-octene

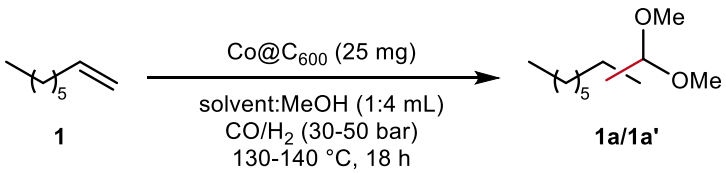

Entry	Catalyst	Solvent	Temperature (°C)	Pressure (bar)	Time (h)	Conv. (%) [b]	Yield **1a/1a'** (%) [b]	**1a/1a'** L/B
1	Co@C_{600}	toluene	140	50	18	90	74	0.86
2	Co@C_{600}	*p*-cymene	140	50	18	87	69	0.89
3	Co@C_{600}	**anisole**	**140**	**50**	**18**	**96**	**81**	**0.82**
4	Co@C_{600}	dimethyl carbonate	140	50	18	83	69	0.83
5	Co@C_{600}	anisole	140	40	18	92	73	0.87
6	Co@C_{600}	anisole	140	30	18	84	60	0.83
7	Co@C_{600}	anisole	130	50	18	80	70	1.00
8	CoO	anisole	140	50	2	97	92	0.79
9	Co_3O_4	anisole	140	50	2	0	-	-
10	CoO [c]	anisole	140	50	2	99	87	n.a.
11	Co_3O_4 [c]	anisole	140	50	2	63	62	n.a.
12	Co@C_{600}	anisole	140	50	4	60	51	0.86
13	Co@C_{600} (from MOF-74)	anisole	140	50	4	98	97	0.80

[a] 1-octene (2 mmol), Co@C_{600} (25 mg), total solvent (5 mL), CO/H_2 (40 bar). [b] Conversion and yield were determined by GC using mesitylene as the internal standard. [c] nonanal (2 mmol) was used as substrate.

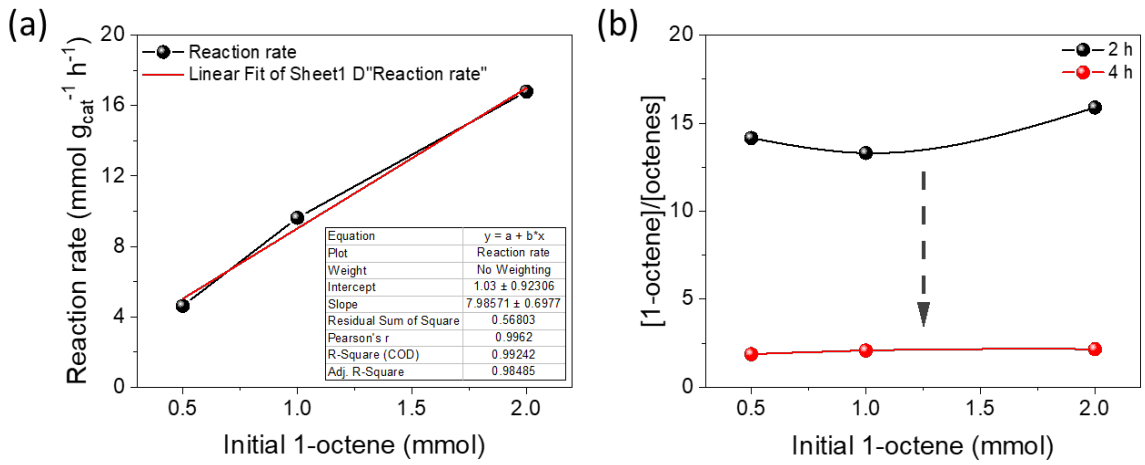

Figure S 8. (a) 1-octene reaction rate and (b) monitoring of octenes formation. Conditions: 1-octene (0.5 - 2 mmol), Co@C_{600} (25 mg), anisole/methanol (5 mL), CO/H_2 (50 bar). Conversion and yield were determined by GC using mesitylene as the internal standard

Reaction rate and [1-octene]/[octenes] were calculated as follows:

$$Reaction\ rate\ (mmol\ g_{cat}^{-1}\ h^{-1}) = \frac{\Delta mmol_{1-octene}}{m_{cat} \times \Delta t}$$

$$\frac{[1-octene]}{[octenes]} = \frac{mmol\ 1-octene_{t=x\ h}}{mmol\ octenes_{t=x\ h}}$$

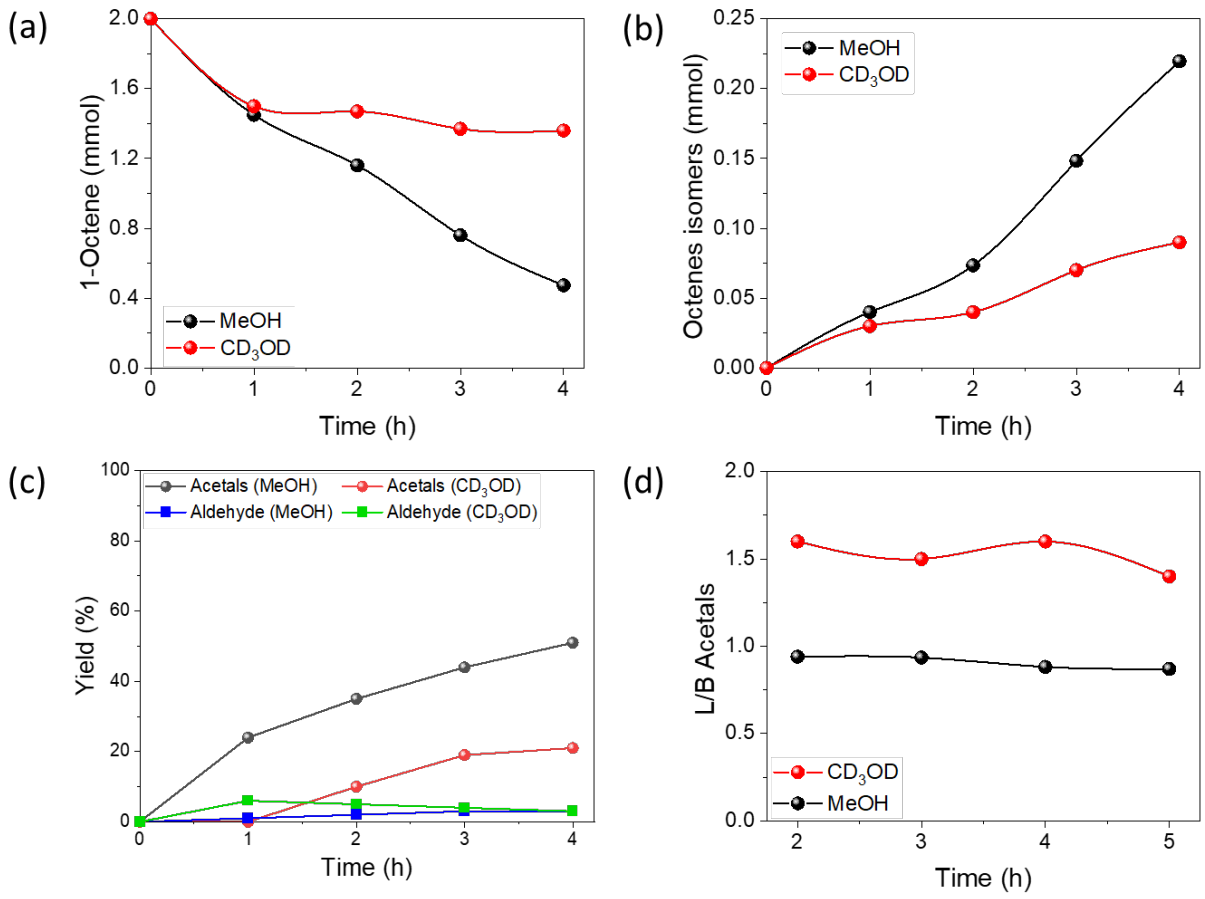

Figure S 9. Kinetic isotope effect experiments with CH_3OH and CD_3OD. (a) 1-octene consumption, (b) formation of internal octenes, (c) acetals and aldehydes yields, and (d) linear-to-branched ratio formation of acetals.

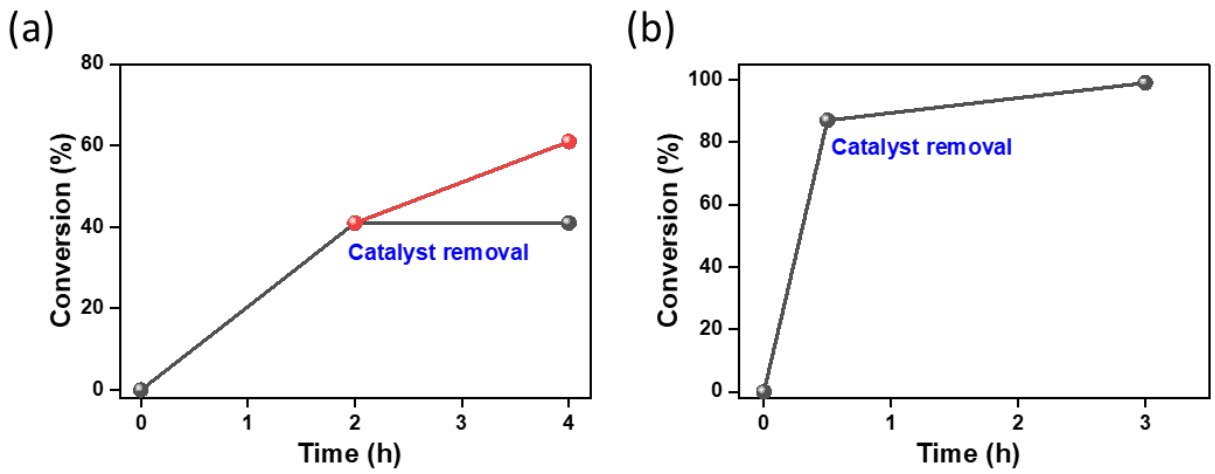

Figure S10. Hot filtration experiment with the (a) Co@C_{600} and (b) pyrolyzed MOF-74 catalysts. Conditions: 1-octene (2 mmol), Co@C_{600} (25 mg), anisole:methanol (1:4 mL), 140 °C, CO/H_2 (50 bar).

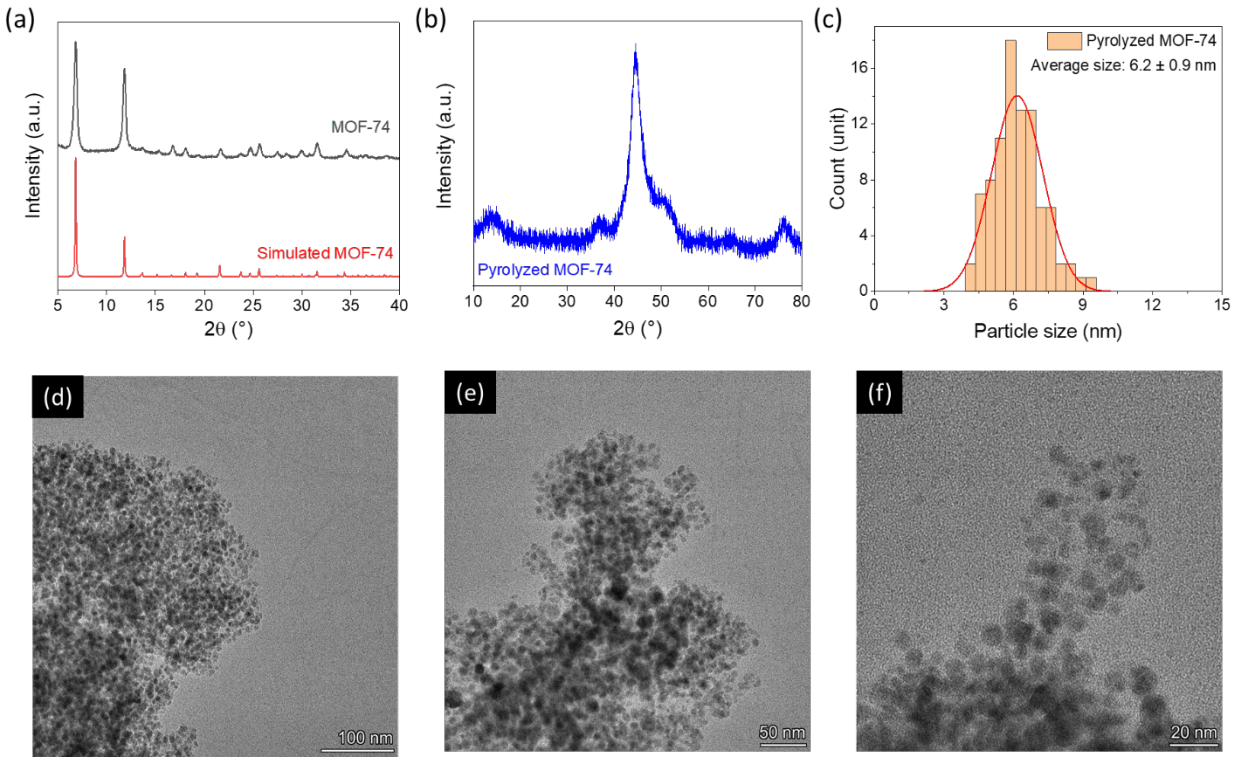

Figure S 11. PXRD of (a) MOF-74 and (b) its pyrolyzed material, (c) cobalt particle size distribution and (d-f) TEM images of pyrolyzed MOF-74.

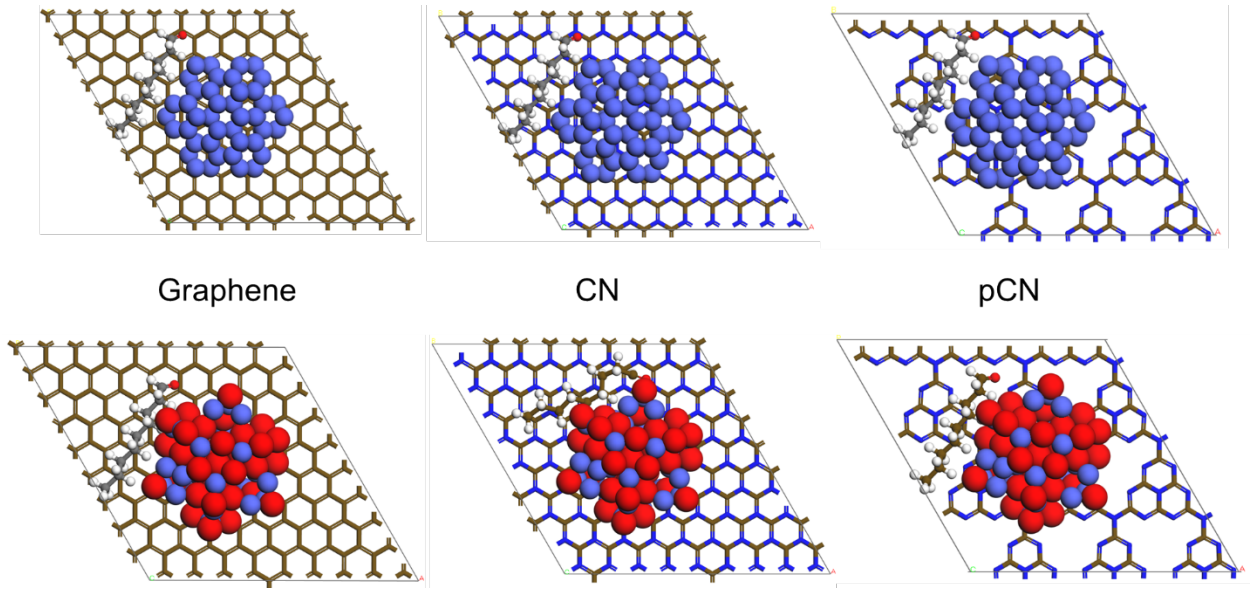

Figure S12. Nonanal adsorption on Co and CoO on supports (Graphene, CN and pCN)

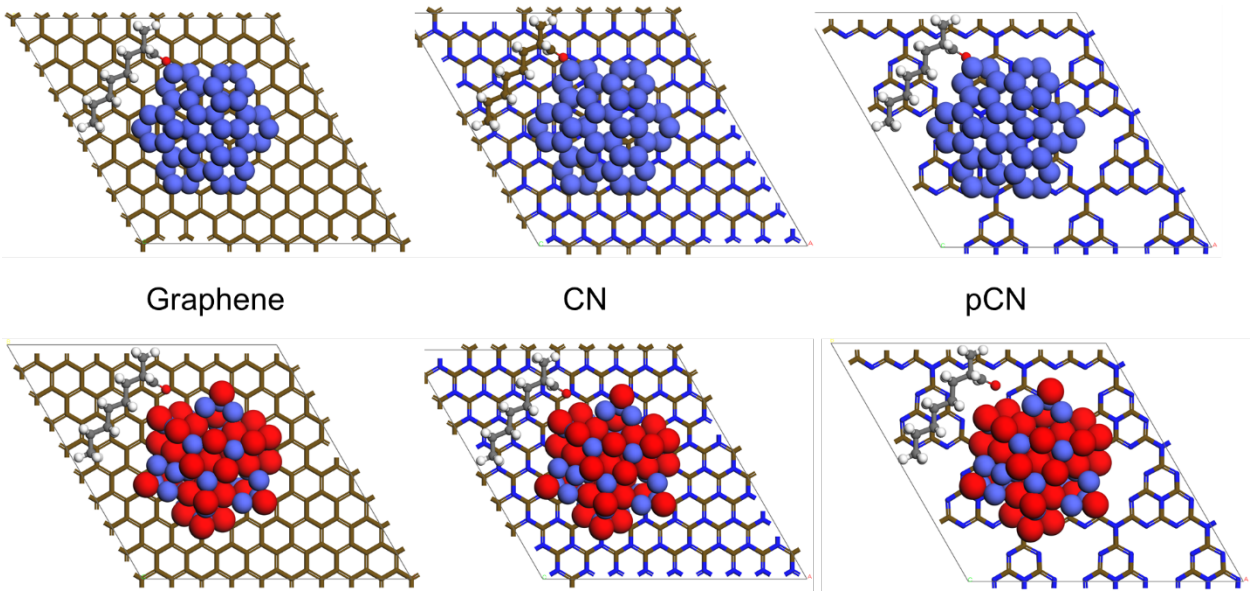

Figure S13. 2-Methyloctanal adsorption on Co and CoO on supports (Graphene, CN and pCN)

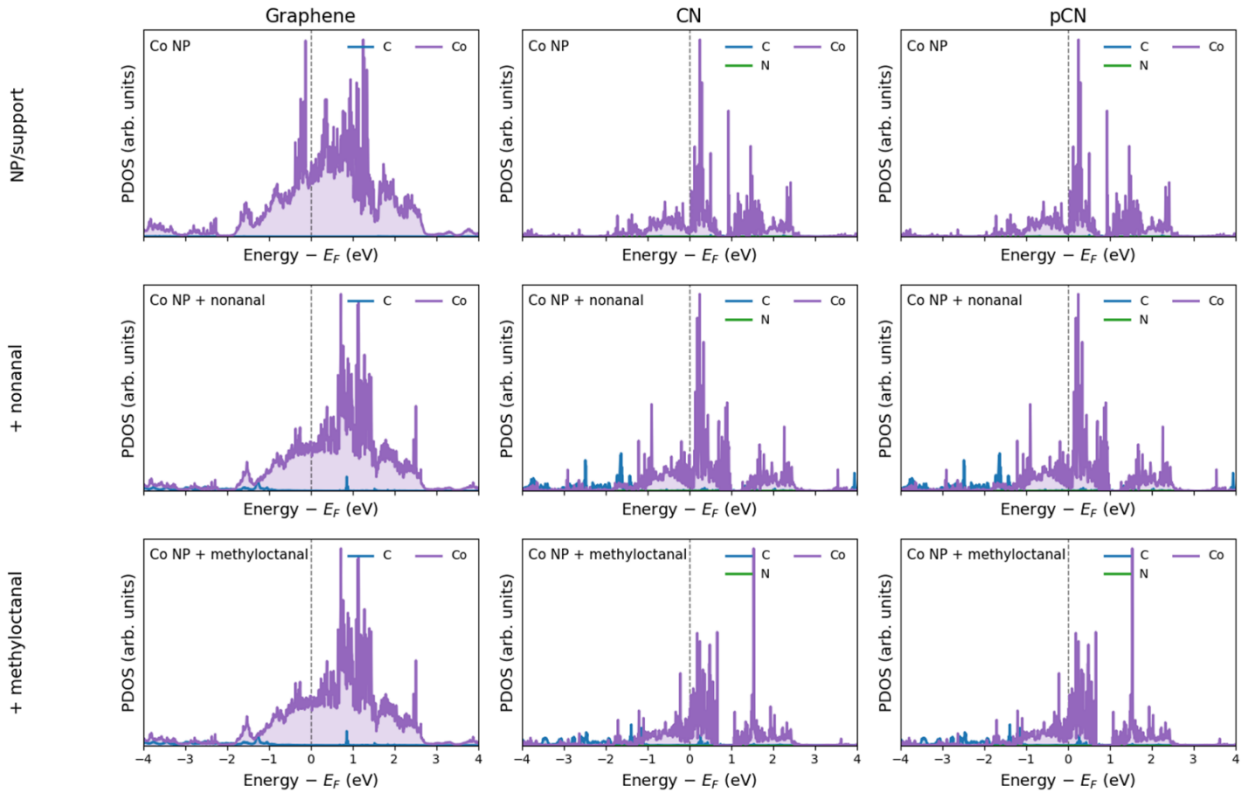

Figure S 14. Element-resolved projected density of states (PDOS) for Co nanoparticles (Co NP) supported on graphene, nitrogen-doped graphene (CN), and porous carbon nitride (pCN) before and after adsorption of nonanal and 2-methyloctanal.

The PDOS illustrates the electronic interaction between the carbon support (C), nitrogen dopants (N), and surface Co atoms. Upon aldehyde adsorption, new states appear near the Fermi level (dashed line), indicating orbital hybridization between Co 3d states and the carbonyl oxygen lone pairs. Nitrogen doping (CN and pCN) increases the electronic density near the Fermi energy, enhancing metal–support interaction and strengthening aldehyde adsorption compared to pristine graphene.

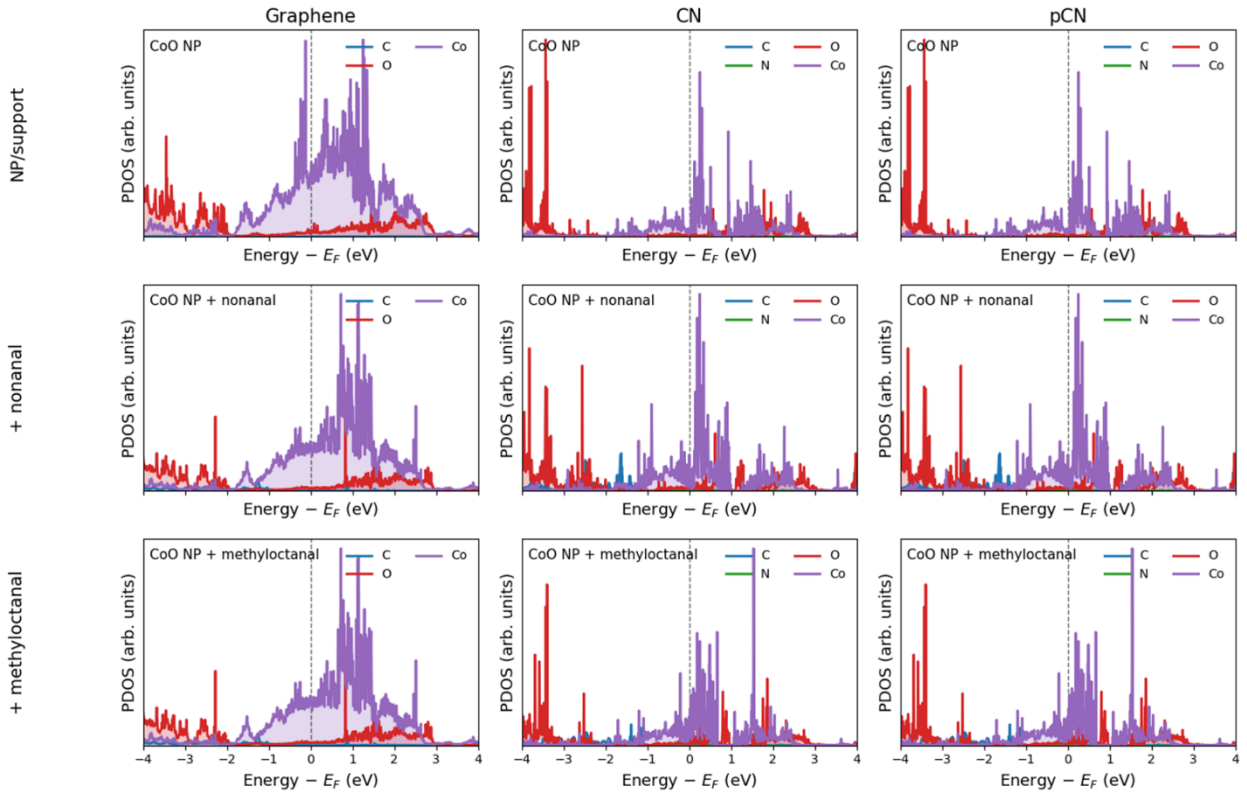

Figure S 15. Element-resolved projected density of states (PDOS) for CoO nanoparticles (CoO NP) supported on graphene, nitrogen-doped graphene (CN), and porous carbon nitride (pCN) before and after adsorption of nonanal and 2-methyloctanal.

The PDOS shows contributions from carbon in the support (C), nitrogen dopants (N), oxygen from the CoO cluster and adsorbates (O), and cobalt (Co). Upon aldehyde adsorption, additional states emerge near the Fermi level (dashed line), indicating Co–O orbital interaction between the carbonyl group and exposed cobalt sites. Nitrogen-containing supports (CN and pCN) exhibit higher DOS intensity around the Fermi level compared to pristine graphene, suggesting stronger metal–support electronic coupling and enhanced adsorption strength on N-doped carbon frameworks.

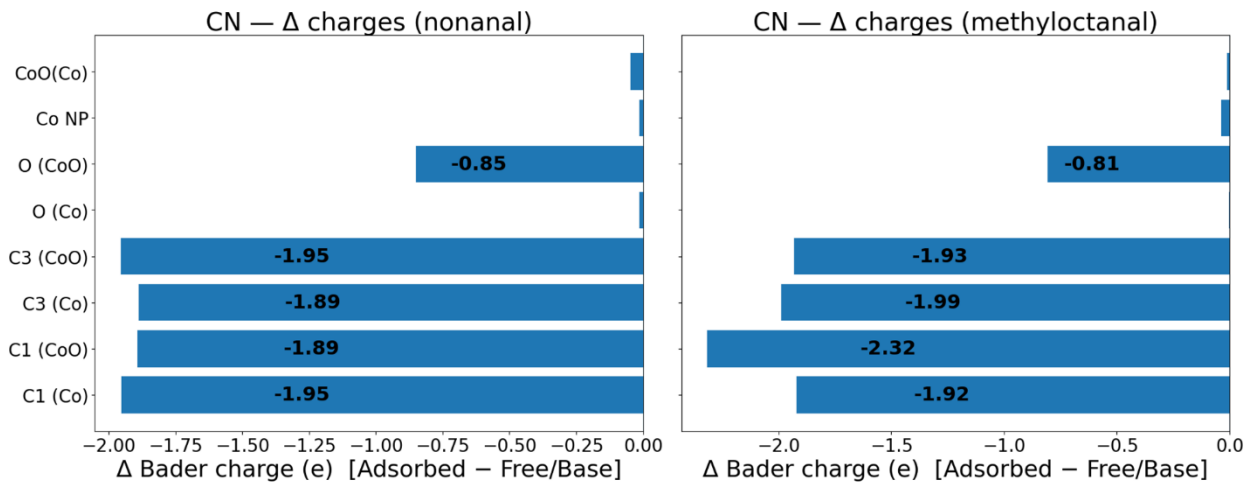

Figure S 16. Changes in Bader charge (Δ charge = adsorbed − free/base) for selected atoms during adsorption of nonanal (left) and 2-methyloctanal (right) on Co and CoO nanoparticles supported on nitrogen-doped graphene (CN).

C1 and C3 correspond to the carbon atoms in the aldehyde backbone closest to the carbonyl group, while O denotes the aldehyde oxygen atom directly interacting with the nanoparticle surface. A small increase in negative charge on the carbonyl oxygen (Δ ≈ –0.8 e) indicates electron donation from the aldehyde to surface Co/CoO sites, while changes on C1 and C3 reflect polarization along the C=O bond upon adsorption. The overall charge redistribution is modest, suggesting that adsorption is dominated by Co–O orbital hybridization rather than large net charge transfer, consistent with chemisorptive interaction.

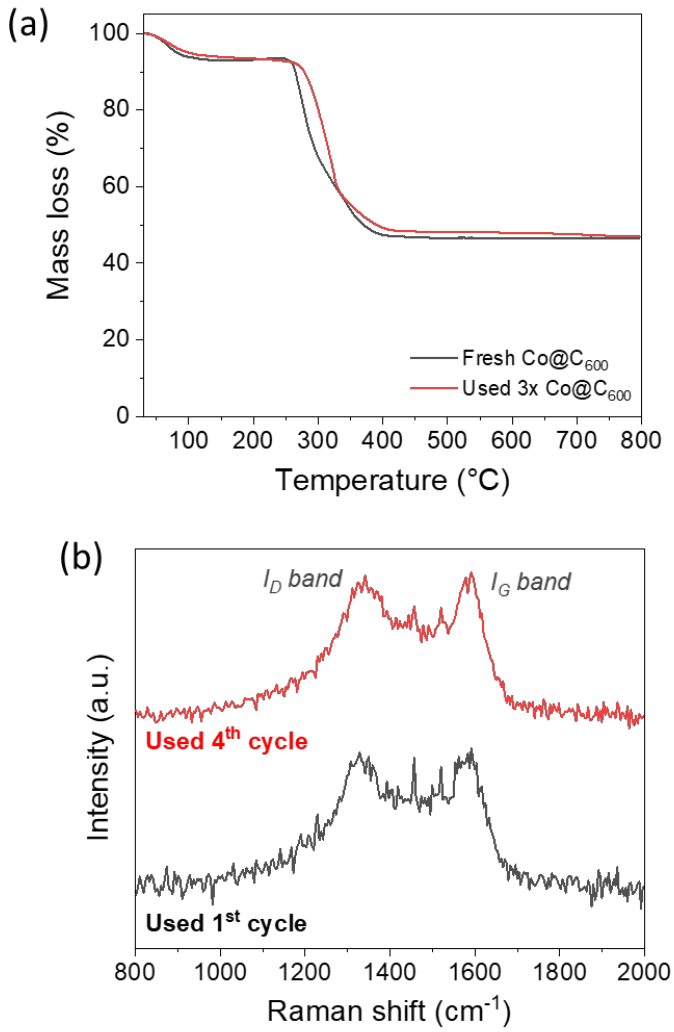

Figure S 17. (a) TGA and (b) Raman spectroscopy of fresh and used Co@C_{600} catalyst

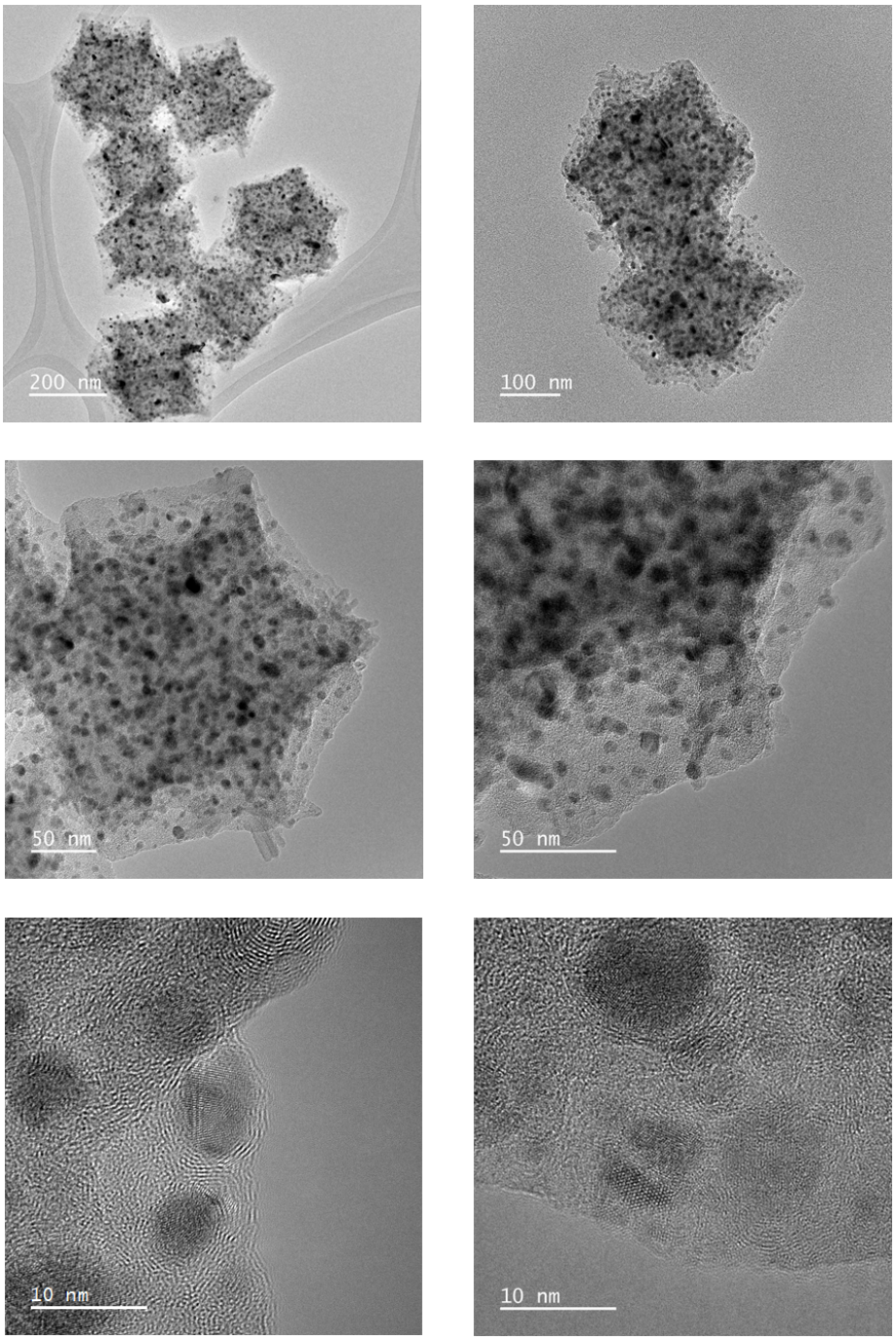

Figure S18. TEM images of used Co@C_{600}

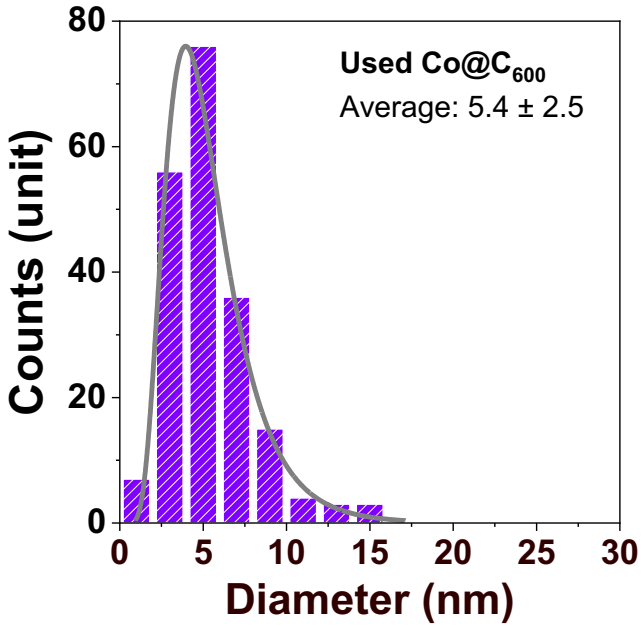

Figure S19. Cobalt particle size distribution of the used Co@C_{600} catalyst

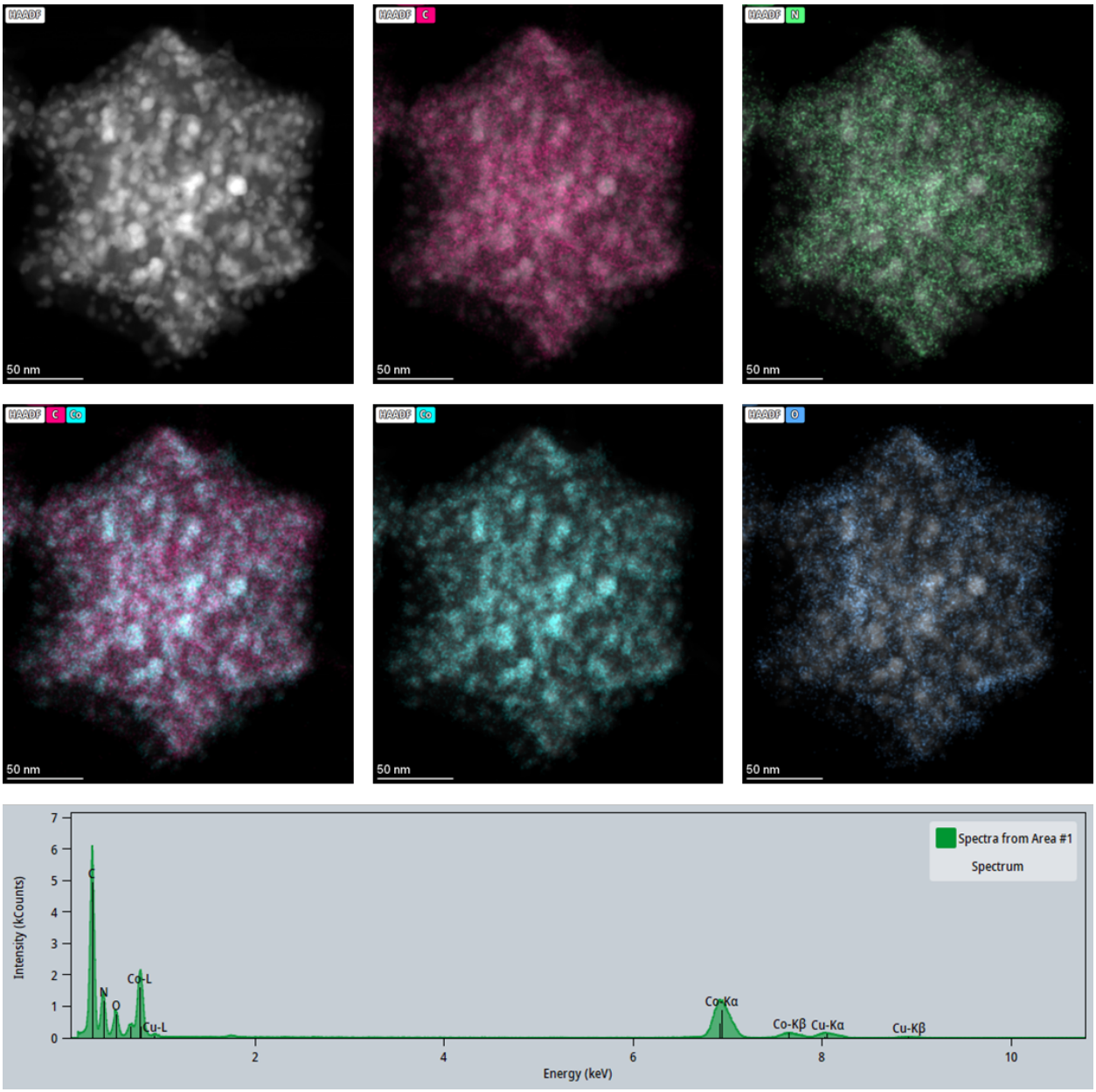

Figure S20. High-angle annular dark-field scanning transmission electron microscopy (HAADF-STEM) of the used Co@C_{600} after five cycles

Table S6. Elemental quantification by XPS

Sample	Atomic percentage (%)			
	Co	N	C	O
Fresh Co@C_{600}	27.5	12.0	46.1	14.4
Used 5x Co@C_{600}	32.0	8.7	42.7	16.6

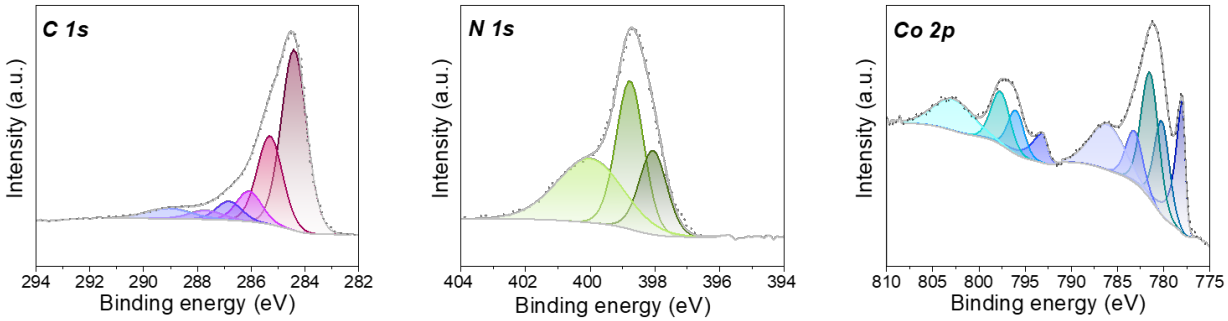

Figure S21. C 1s, N 1s, and Co 2p XPS spectra of the used Co@C_{600} catalyst.

Table S 7. O 1s XPS deconvolution data

Species	Binding energy (eV)	Composition (%)	
		Fresh	Used 5x
Co-O (lattice)	530.0	6.70	3.50
C=O	531.2	27.6	26.3
Co-OH (defective oxygen)	532.1	31.9	45.8
COOH (ads)	533.5	33.7	24.3

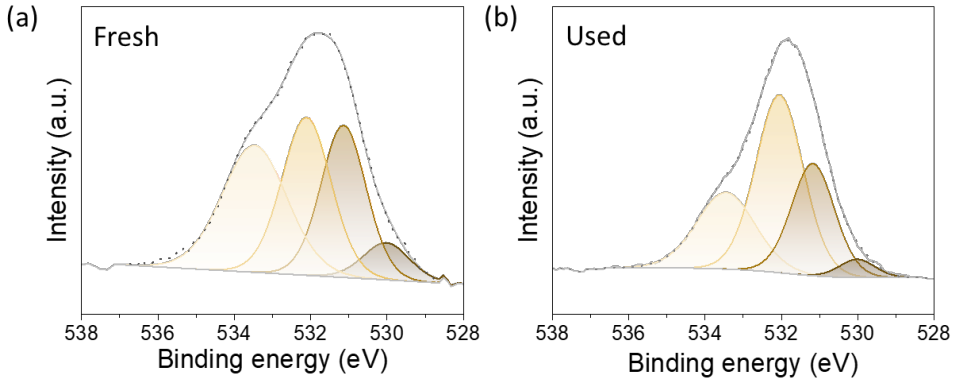

Figure S 22. O 1s XPS spectra of (a) fresh and (b) used Co@C_{600} catalyst

References

1 L. Garzón-Tovar, A. Carné-Sánchez, C. Carbonell, I. Imaz and D. Maspoch, *J. Mater. Chem. A*, 2015, **3**, 20819–20826.